Automatica, Volume 145, November 2022, Article number 110561
DOI:10.1016/j.automatica.2022.110561

Attitude Tracking Control for Reentry Vehicles using Centralised Robust Model Predictive Control

Runqi Chai [a], Antonios Tsourdos [b], Huijun Gao [c], Senchun Chai [a], Yuanqing Xia [a]

[a] *School of Automation, Beijing Institute of Technology, Beijing 100081, China*

[b] *School of Aerospace, Transport and Manufacturing, Cranfield University, Cranfield MK43 0AL, UK*

[c] *Research Institute of Intelligent Control and Systems, Harbin Institute of Technology, Harbin 150001, China*

Abstract

In this work, a centralised robust model predictive control (CRMPC) algorithm is proposed for reentry vehicles to track reference attitude trajectories subject to state/input constraints and uncertainties. In contrast to most designs that apply a cascade control structure for the two-timescale attitude dynamical systems, the proposed control scheme utilises a centralised structure to avoid additional controller development and parameter turning. By designing a nonlinear feedback law and tightening the system constraints, robust constraint satisfaction can be ensured for all admissible uncertainties. In addition, to guarantee the recursive feasibility and closed-loop stability of the proposed CRMPC, a terminal controller, along with a terminal region, is introduced. The validity of using the proposed approach to solve the considered problem is confirmed by executing several experimental studies, which were compared against two other established methods.

Key words: Robust model predictive control; reentry vehicle; attitude tracking; nonlinear feedback law.

1 Introduction

Attitude control system development for aerospace vehicles (e.g., unmanned aerial vehicles, reentry vehicles, and reusable rockets) has long been recognised as a popular research area owing to its extensive applications in numerous engineering problems such as the reentry flight [22], rendezvous and docking [4, 6], and satellite formation flying [19], among others. Commonly, the main objective of developing an attitude control system is to provide the vehicle with reference tracking or attitude stabilisation capabilities. By investigating the spacecraft control process, it is evident that the corresponding attitude dynamics can be characterised by a multi-timescale system. This is because the angular-rate variables typically undergo faster changes than angular variables. A widely acceptable strategy for the control of such a multirate system is to resort to the timescale separation technique. Specifically, the spacecraft attitude system is divided into two interacting subsystems: a slow outer angular subsystem and a fast inner angular-rate subsystem. Then, robust controllers are designed for these two subsystems. Previous studies have verified that certain advantages can be acquired from employing this hierarchical control structure [16]. For example, provided that the inner loop is typically faster than the outer loop, the entire system tends to be more effective at responding to disturbances. More importantly, it has the potential to reduce the degree of variability within the process. Some studies focused on developing multirate controllers for spacecraft attitude tracking problems have been published in recent years [14, 20]. Among these contributions, the application of sliding mode control (SMC) appears to be a popular choice and is highly regarded by researchers. For example, Tian et al.[20] addressed the problem of reusable launch vehicle reentry attitude tracking by applying a double-layered second-order SMC algorithm. In their follow-up research [14], the possibility of utilising a double-layered fuzzy-disturbance observer-based adaptive SMC algorithm to track desired attitude signals was explored. Although simulation results demonstrated that the attitude-tracking task can be successfully accomplished, how to balance the high-frequency chattering effects and the control accuracy remains an open issue. Apart from this algorithm-related drawback, there are some

Email addresses: r.chai@bit.edu.cn (Runqi Chai), a.tsourdos@cranfield.ac.uk (Antonios Tsourdos), hjgao@hit.edu.cn (Huijun Gao), chaisc97@163.com (Senchun Chai), xia_yuanqing@bit.edu.cn (Yuanqing Xia).

concerns regarding the structure of the controllers [10, 21]. Because most of these aforementioned works employ a cascaded two-level design, additional measurement of the inner-loop variables is required, which eventually doubles the instrumentation costs. Besides, the control strategy tends to become more complex, as additional controller development is required for the inner loop. Furthermore, to achieve a satisfactory control performance, an additional parameter-tuning process is necessary for the inner and outer controllers.

To avoid these drawbacks, centralised robust controllers have been proposed by some researchers [3, 7, 25]. A resilient attitude-control scheme was developed by [3], who utilised a nonlinear observer to reject the effect caused by disturbances such that the tracking performance can be improved. Similarly, Zhang et al. (2019) developed a disturbance observer along with an integral SMC method [7] to form a centralised attitude controller. Although using these centralised controllers allows for acceptable attitude-tracking performance, the system constraints such as the state/input limitations were not fully considered, which may have non-negligible impacts on engineering practices. In this paper, we describe our attempt to design a robust model predictive control (RMPC)-based attitude-tracking control scheme so as to generate tracking control actions for reentry vehicles in the presence of constraints and external uncertainties. RMPC is a widely-engaged process-control strategy owing to its guaranteed constraint handling ability and enhanced anti-disturbance performance. It has been applied in various industrial applications including smart grids [17], intelligent transport systems [18], space explorations [13], and robotics [15]. In the context of aerospace vehicle motion or attitude control, several RMPC-oriented contributions have been made during the last decade [2, 9, 12, 23]. For instance, [12] investigated the tube technique and developed an RMPC scheme to regulate the linearised CubeSat attitude system during an Earth observation mission. [23] considered the attitude control problem for spacecraft with single gimbal control moment gyros by combining model predictive control (MPC) with the H_∞ technique to form a dual-mode control law. One advantage of such a design is that the resulting control action has an extra degree of freedom to compensate for the negative effect caused by the uncertainties. In addition, a robust three-axis spacecraft attitude-tracking problem was considered by [2], who combined SMC and linear MPC to produce the optimal tracking control profiles. Based on the obtained simulation results, the authors verified that such a compound control scheme is able to steer the attitude motion to follow the desired references. However, more effort is required to develop the additional controllers and tune the algorithm-related parameters. In addition, the actual control performance can be easily affected owing to poor treatment of these additional processes. In terms of its structure, the proposed CRMPC scheme is centralised without separating the two-timescale-attitude dynamical systems, thus simultaneously determining all the manipulated variables. Compared to some of the existing designs (e.g., [2, 14, 20, 24]), the proposed scheme has simplified the structure of the controller. Only one optimisation-based control loop is required instead of a double-layered control framework. Hence, controller development and parameter tuning for the fast inner layer (i.e., angular rate system) can be avoided. More specifically, the main contributions of this work can be summarised as follows. First, a new CRMPC algorithm is established for reentry vehicles to track desired angular profiles in the presence of state/input constraints and uncertainties; second, we made progress towards developing a nonlinear feedback law, tightened system constraints, and a terminal controller with corresponding terminal region such that robust constraint satisfaction can be achieved, thereby confirming the recursive feasibility and input-to-state stability (ISS) of the proposed CRMPC. Third, experiments were performed to validate the effectiveness of the proposed attitude-tracking controller. The performances of other well-developed multirate controllers were compared to evaluate the merit of our centralised design.

2 Description of System Equations

Notation: The real space and n-dimensional Euclidean space are denoted as $\mathbb{R}$ and $\mathbb{R}^n$, respectively. $\text{diag}\{a_1, ..., a_n\}$ represents the diagonal matrix, where $a_1, ..., a_n$ are its elements. Define $\mathbf{a} = [a_1, ..., a_n]^T$ as a vector, then $|\mathbf{a}| = [|a_1|, ..., |a_n|]^T$, $\|\mathbf{a}\| = \sqrt{\mathbf{a}^T\mathbf{a}}$ and $\|\mathbf{a}\|_P = \sqrt{\mathbf{a}^T\mathbf{P}\mathbf{a}}$, in which $\mathbf{P}$ is a positive definite matrix. Let $\mathbf{M} \in \mathbb{R}^{n\times n}$, then its 2-norm is defined as $\|\mathbf{M}\| = \sqrt{\lambda_{\max}(\mathbf{M}^T\mathbf{M})}$, in which $\lambda_{\max}$ represents the maximum eigenvalue. Similarly, $\lambda_{\min}$ is the minimum eigenvalue. Let $\mathbb{A} \subset \mathbb{R}^n$ and $\mathbb{B} \subset \mathbb{R}^n$ denote two sets, then $\mathbb{A} \oplus \mathbb{B} = \{m + n | m \in \mathbb{A}, n \in \mathbb{B}\}$ and $\mathbb{A} \ominus \mathbb{B} = \{z \in \mathbb{R}^n | \{z\} \oplus \mathbb{B} \subset \mathbb{A}\}$.

2.1 Rotational Equations of Motion

The rotational motion of the reentry vehicle can be described by the following matrix representation [5, 8, 20]:

$$\begin{cases} \dot{\boldsymbol{\Theta}} = \boldsymbol{R}\boldsymbol{\omega} + \boldsymbol{\Delta}_f & \text{(1a)} \\ \dot{\boldsymbol{\omega}} = -\boldsymbol{I}^{-1}\boldsymbol{\Omega}\boldsymbol{I}\boldsymbol{\omega} + \boldsymbol{I}^{-1}\mathbf{m} + \boldsymbol{\Delta}_m & \text{(1b)} \end{cases}$$

where the matrix terms $\boldsymbol{R}$, $\boldsymbol{I}$, and $\Omega \in \mathbb{R}^{3\times3}$ are given by

$$\boldsymbol{R} = \begin{bmatrix} -\cos\alpha\tan\beta & 1 & -\sin\alpha\tan\beta \\ \sin\alpha & 0 & -\cos\alpha \\ -\cos\alpha\cos\beta & -\sin\beta & -\cos\beta\sin\alpha \end{bmatrix}. \quad (2)$$

$$\boldsymbol{I} = \begin{bmatrix} I_{xx} & -I_{xy} & -I_{xz} \\ -I_{yx} & I_{yy} & -I_{yz} \\ -I_{zx} & -I_{zy} & I_{zz} \end{bmatrix}, \boldsymbol{\Omega} = \begin{bmatrix} 0 & -\nu & q \\ \nu & 0 & -p \\ -q & p & 0 \end{bmatrix}. \quad (3)$$

In (1)-(3), $\boldsymbol{\Theta} = [\alpha, \beta, \sigma]^T$ denotes the attitude-angle vector in the earth-fixed coordinate frame. Because reentry vehicles are the intended application, $\boldsymbol{\Theta}$ consists of the angle of attack α, sideslip angle β and bank angle σ. $\boldsymbol{\omega} = [p, q, \nu]^T$ represents the angular-rate vector in the body-fixed coordinate frame, where the roll rate is p, pitch rate is q, and yaw rate is ν, respectively. The control moment vector is denoted as $\mathbf{m} = [m_x, m_y, m_z]^T$. $m_i, i = (x, y, z)$ represents the roll, pitch, and yaw moment, whilst I_{ij}, $(i, j = x, y, z)$ is the roll, pitch, and yaw moment of inertia. $\boldsymbol{\Delta}_f$, $\boldsymbol{\Delta}_m \in \mathbb{R}^{3\times 1}$ are considered as additive disturbances owing to environmental uncertainties and model simplification.

If we redefine the system state and control variable as $\boldsymbol{x} = [\boldsymbol{x}_\Theta, \boldsymbol{x}_\omega]^T \in \mathbb{R}^{6\times 1}$ and $\boldsymbol{u} = \boldsymbol{R}\boldsymbol{I}^{-1}\mathbf{m} \in \mathbb{R}^{3\times 1}$, with $\boldsymbol{x}_\Theta = \boldsymbol{\Theta}$ and $\boldsymbol{x}_\omega = \boldsymbol{R}\boldsymbol{\omega} + \boldsymbol{\Delta}_f$, then system (1) is rewritten as follows:

$$\begin{cases} \dot{\boldsymbol{x}}_\Theta = \boldsymbol{x}_\omega & (4a) \\ \dot{\boldsymbol{x}}_\omega = \dot{\boldsymbol{R}}(\boldsymbol{\Theta})\boldsymbol{\omega} - \boldsymbol{R}(\boldsymbol{\Theta})\boldsymbol{I}^{-1}\boldsymbol{\Omega}(\omega)\boldsymbol{I}\boldsymbol{\omega} + \boldsymbol{u} + \boldsymbol{\Delta} & (4b) \end{cases}$$

with $\boldsymbol{\Delta} = \dot{\boldsymbol{\Delta}}_f + \boldsymbol{R}\boldsymbol{\Delta}_m$.

Some preliminary assumptions are made to develop the proposed optimisation-based tracking controller.

Assumption 1 *The attitude angle $\boldsymbol{\Theta}$, angular rate $\boldsymbol{\omega}$, and control variables $\mathbf{m}$ are assumed to be measurable.*

Assumption 2 *The disturbance terms $\boldsymbol{\Delta}_f$, $\boldsymbol{\Delta}_m$ together with their first-order derivatives are bounded. Moreover, it is supposed that there exist upper bounds on $\boldsymbol{\Delta}$, that is, $\|\boldsymbol{\Delta}\| \leq \bar{\Delta}$.*

Assumption 3 *The attitude-angle references, together with their first- and second-order derivatives, are considered to be smooth and bounded, i.e., $\|\boldsymbol{\Theta}_r\| \leq \bar{\Theta}_0$, $\|\dot{\boldsymbol{\Theta}}_r\| \leq \bar{\Theta}_1$, and $\|\ddot{\boldsymbol{\Theta}}_r\| \leq \bar{\Theta}_2$.*

Assumption 4 *The inertia matrix $\boldsymbol{I}$ and its inverse matrix are assumed to be bounded, i.e., $\|\boldsymbol{I}\| \leq \bar{I}$ and $\|\boldsymbol{I}^{-1}\| \leq \bar{I}^{'}$.*

Assumption 2 is widely applied in designing attitude controller for reentry vehicles [8, 14, 20]. Specifically, based on the expressions of $\boldsymbol{\Delta}_f$ and $\boldsymbol{\Delta}_m$ (see e.g., Eq. (8) of [8]), one can observe that all their elements and first-order derivatives can be bounded in a real flight scenario. Hence, Assumption 2 is reasonable. For space reasons, the expressions of $\boldsymbol{\Delta}_f$ and $\boldsymbol{\Delta}_m$ are omitted here. Interested readers can refer to [8] for more details.

2.2 Tracking Error Dynamics

If we further define the attitude-tracking error vector as $\mathbf{E} = [\mathbf{E}_\theta, \mathbf{E}_\omega]^T \in \mathbb{R}^{6\times 1}$, in which $\mathbf{E}_\theta = \boldsymbol{\Theta} - \boldsymbol{\Theta}_r$ and $\mathbf{E}_\omega = \boldsymbol{R}\boldsymbol{\omega} - \dot{\boldsymbol{\Theta}}_r$, then it can model the tracking error dynamics in the form of

$$\begin{cases} \dot{\mathbf{E}}_\theta = \mathbf{E}_\omega & (5a) \\ \dot{\mathbf{E}}_\omega = \dot{\boldsymbol{R}}(\boldsymbol{\Theta})\boldsymbol{\omega} - \boldsymbol{R}(\boldsymbol{\Theta})\boldsymbol{I}^{-1}\boldsymbol{\Omega}(\boldsymbol{\omega})\boldsymbol{I}\boldsymbol{\omega} + \boldsymbol{u} - \ddot{\boldsymbol{\Theta}}_r + \boldsymbol{\Delta} & (5b) \end{cases}$$

Hence, the primary objective of the tracking controller becomes steering the actual angle profiles to track the references, while simultaneously guaranteeing the variable constraints $\boldsymbol{x}_\omega \in \mathbb{X}_\omega$ and $\boldsymbol{u} \in \mathbb{U}_m$. Here, the variable admissible sets $\mathbb{X}_\omega$ and $\mathbb{U}_m$ are defined as follows:

$$\begin{aligned} \mathbb{X}_\omega &= \{\boldsymbol{x}_\omega \in \mathbb{R}^{3\times 1} : \|\boldsymbol{x}_\omega\| \leq \bar{x}_\omega\} \\ \mathbb{U}_m &= \{\boldsymbol{u} \in \mathbb{R}^{3\times 1} : \|\boldsymbol{u}\| \leq \bar{u}\} \end{aligned} \quad (6)$$

in which $\bar{x}_\omega > 0$ and $\bar{u} > 0$ denote the bounds of $\boldsymbol{x}_\omega$ and $\bar{u}$. A nominal form of the system dynamics (4) is obtained when the external disturbances are omitted, which can be described as follows:

$$\begin{cases} \dot{\tilde{\boldsymbol{x}}}_\Theta = \tilde{\boldsymbol{x}}_\omega & (7a) \\ \dot{\tilde{\boldsymbol{x}}}_\omega = \dot{\boldsymbol{R}}(\tilde{\boldsymbol{\Theta}})\tilde{\boldsymbol{\omega}} - \boldsymbol{R}(\tilde{\boldsymbol{\Theta}})\boldsymbol{I}^{-1}\boldsymbol{\Omega}(\tilde{\boldsymbol{\omega}})\boldsymbol{I}\tilde{\boldsymbol{\omega}} + \tilde{\boldsymbol{u}} & (7b) \end{cases}$$

Here, $\tilde{\boldsymbol{\Theta}}$ and $\tilde{\boldsymbol{\omega}}$ are the nominal attitude angle and angular-rate vectors, respectively.

The nominal tracking error dynamics can then be written as

$$\begin{cases} \dot{\tilde{\mathbf{E}}}_\theta = \tilde{\mathbf{E}}_\omega & (8a) \\ \dot{\tilde{\mathbf{E}}}_\omega = \dot{\boldsymbol{R}}(\tilde{\boldsymbol{\Theta}})\tilde{\boldsymbol{\omega}} - \boldsymbol{R}(\tilde{\boldsymbol{\Theta}})\boldsymbol{I}^{-1}\boldsymbol{\Omega}(\tilde{\boldsymbol{\omega}})\boldsymbol{I}\tilde{\boldsymbol{\omega}} + \tilde{\boldsymbol{u}} - \ddot{\boldsymbol{\Theta}}_r & (8b) \end{cases}$$

The next lemma reveals that with proper specification of variable ranges, some basic properties hold true for $\boldsymbol{R}$, $\boldsymbol{R}^{-1}$, $\boldsymbol{I}$, and $\boldsymbol{\Omega}$.

Lemma 1 *For any $\beta \in (-\frac{\pi}{2}, \frac{\pi}{2})$ and bounded $\boldsymbol{\omega}$, there exist upper and lower bounds for the 2-norm of $\boldsymbol{R}$, $\boldsymbol{R}^{-1}$, $\dot{\boldsymbol{R}}$, and $\boldsymbol{\Omega}$, that is, $\underline{r}_0 \leq \|\boldsymbol{R}(\boldsymbol{\Theta})\| \leq \bar{r}_0$, $\underline{r}_1 \leq \|\dot{\boldsymbol{R}}(\boldsymbol{\Theta})\| \leq \bar{r}_1$, $\underline{r}_0^{'} \leq \|\boldsymbol{R}^{-1}(\boldsymbol{\Theta})\| \leq \bar{r}_0^{'}$, and $\|\boldsymbol{\Omega}(\boldsymbol{\omega})\| \leq \bar{\Omega}$.*

PROOF. The 2-norm of $\boldsymbol{R}(\boldsymbol{\Theta})$ is defined as $\|\boldsymbol{R}(\boldsymbol{\Theta})\| = \sqrt{\lambda_{\max}(\boldsymbol{R}^T\boldsymbol{R})}$. According to the Sylvester's determinant theorem [1], $\boldsymbol{R}\boldsymbol{R}^T$ and $\boldsymbol{R}^T\boldsymbol{R}$ have the same nonzero eigenvalues. By solving $|\lambda\mathbf{I}_3 - \boldsymbol{R}\boldsymbol{R}^T| = 0$, it is found that $\lambda_1 = \tan^2\beta + 1$, $\lambda_2 = \lambda_3 = 1$. Here $\mathbf{I}_3$ denotes the 3×3 identity matrix. Consequently, for any $|\beta| \neq \frac{\pi}{2}$, the bounds of $\|\boldsymbol{R}(\boldsymbol{\Theta})\|$ are $\underline{r}_0 = 1$ and $\bar{r}_0 = \sqrt{\tan^2\beta + 1}$, respectively. For $\dot{\boldsymbol{R}}$, its expression is derived as

$$\frac{d\boldsymbol{R}(\boldsymbol{\Theta})}{dt} = \begin{bmatrix} \dot{\alpha}\tan\beta\sin\alpha - \dot{\beta}\frac{\cos\alpha}{\cos^2\beta} & 0 & -\dot{\alpha}\cos\alpha\cos\beta - \dot{\beta}\frac{\sin\alpha}{\cos^2\beta} \\ \dot{\alpha}\cos\alpha & 0 & \dot{\alpha}\sin\alpha \\ \dot{\alpha}\sin\alpha\cos\beta & -\dot{\beta}\cos\beta & -\dot{\alpha}\cos\alpha\cos\beta + \dot{\beta}\sin\alpha\sin\beta \end{bmatrix}$$

Denoting $\mathbf{A}_1 = \frac{d\boldsymbol{R}}{dt}\left(\frac{d\boldsymbol{R}}{dt}\right)^T$, it is calculated that $\mathbf{A}_1 = \mathrm{diag}\{a_{11}, a_{22}, a_{33}\}$, where $a_{11} = \sec^2\beta(\dot{\alpha}^2\sin^2\beta + \dot{\beta}^2\sec\beta)$, $a_{22} = \dot{\alpha}^2$ and $a_{33} = \dot{\alpha}\cos^2\beta + \dot{\beta}^2$, respectively. As $\|\boldsymbol{R}\|$, $\boldsymbol{\omega}$ are bounded and $|\beta| \neq \frac{\pi}{2}$, the bounds of $\|\dot{\boldsymbol{R}}\| = \sqrt{\lambda_{\max}(\mathbf{A}_1)}$, exist and can be determined correspondingly. In addition, from (2), $\boldsymbol{R}^{-1}$ can be written as

$$\boldsymbol{R}^{-1}(\boldsymbol{\Theta}) = \begin{bmatrix} -\sin\beta\cos\alpha\cos\beta & \sin\alpha & -\cos\beta\cos\alpha \\ \cos^2\beta & 0 & -\sin\beta \\ -\sin\alpha\cos\beta\sin\beta & -\cos\alpha & -\cos\beta\sin\alpha \end{bmatrix}$$

To calculate its 2-norm (e.g., $\sqrt{\lambda_{\max}((\boldsymbol{R}^{-1})^T)\boldsymbol{R}^{-1}}$), we solve the equation $|\lambda\mathbf{I}_3 - (\boldsymbol{R}^{-1})^T\boldsymbol{R}^{-1}| = 0$. It is obtained that $\lambda_1 = \cos^2\beta$, $\lambda_2 = \lambda_3 = 1$, resulting in $\underline{r}_0^{'} = \bar{r}_0^{'} = 1$. Last, for matrix $\boldsymbol{\Omega}$, by calculating $|\lambda\mathbf{I} - \boldsymbol{\Omega}^T\boldsymbol{\Omega}| = 0$, we find that $\lambda_1 = \lambda_2 = \nu^2 + p^2 + q^2$, and $\lambda_3 = 0$. Hence, for bounded $\boldsymbol{\omega}$, we have $\|\boldsymbol{\Omega}\| \leq \bar{\Omega}$, where $\bar{\Omega} = \sqrt{\arg\max(\nu^2 + p^2 + q^2)}$, which completes the proof.

Remark 1 *In Lemma 1, $\boldsymbol{R}$ and $\dot{\boldsymbol{R}}$ turn out to be singular when $\beta = \pm\frac{\pi}{2}$. Because the purpose of this work is attitude control of reentry vehicles, which usually move in the denser air closer to the Earth than what is commonly recognised as space, maintaining a zero sideslip angle β during the entire flight mission becomes important. Hence, the cases $\beta = \pm\frac{\pi}{2}$ are excluded.*

In following sections, for simplicity, we abbreviate systems (4) and (7) as $\dot{\boldsymbol{x}} = f(\boldsymbol{x}(t), \boldsymbol{u}(t))$ and $\dot{\tilde{\boldsymbol{x}}} = f(\tilde{\boldsymbol{x}}(t), \tilde{\boldsymbol{u}}(t))$, respectively.

3 CRMPC Control Scheme

In this section, a novel CRMPC control algorithm is constructed. The designed MPC scheme does not separate the two-timescale attitude dynamical system (1a) and (1b). Alternatively, it employs a centralised structure, thereby determining all the manipulated variables simultaneously. Before describing the CRMPC algorithm, the primary objectives of the controller are specified.

3.1 Control Objectives

This study aims to construct a centralised optimisation-based controller for the reentry-vehicle attitude system (4) such that the following two individual objectives can be fulfilled:

- The actual attitude-angle profiles should track the desired reference trajectories $\boldsymbol{\Theta}_r = [\alpha_r, \beta_r, \sigma_r]^T$ with the consideration of unknown disturbances $\boldsymbol{\Delta}$.
- The angular-rate variables $\boldsymbol{\omega}$, together with the control moments $\mathbf{m}$, should stay within their admissible sets during the entire tracking process.

The present paper only considers unknown disturbances $\boldsymbol{\Delta}_m$ appearing in the control channel, i.e, $\boldsymbol{\Delta}_f = 0$. The extension of CRMPC for the reentry vehicle subject to unmatched disturbances can be addressed in future research.

3.2 CRMPC Optimization Model

In the proposed CRMPC, attitude tracking is fulfilled by executing two steps. First, an open-loop optimisation model established on the nominal system is iteratively addressed. Subsequently, the resulting optimized state and control pairs are applied to determine the actual control input. To construct the optimisation model, a cost function measuring the tracking performance over the time period $[t_k, t_k + T]$ is designed as follows:

$$\begin{aligned} J_\Phi(\tilde{\mathbf{E}}(t_k), \tilde{\mathbf{U}}_e(t_k)) =& g_\Phi(\tilde{\mathbf{E}}(t_k + T|t_k)) \\ & \int_{t_k}^{t_k+T} L_\Phi(\tilde{\mathbf{E}}(\tau|t_k), \tilde{\mathbf{U}}_e(\tau|t_k))d\tau \end{aligned} \tag{9}$$

with $\tilde{\mathbf{U}}_e$ in the form of

$$\begin{aligned} \tilde{\mathbf{U}}_e &= \dot{\tilde{\mathbf{E}}}_\omega \\ &= \dot{\boldsymbol{R}}(\tilde{\boldsymbol{\Theta}})\tilde{\boldsymbol{\omega}} - \boldsymbol{R}(\tilde{\boldsymbol{\Theta}})\boldsymbol{I}^{-1}\boldsymbol{\Omega}(\tilde{\boldsymbol{\omega}})\boldsymbol{I}\tilde{\boldsymbol{\omega}} + \tilde{\boldsymbol{u}} - \ddot{\boldsymbol{\Theta}}_r \end{aligned}$$

In (9), T stands for the prediction horizon. The terminal cost is given by $g_\Phi = \|\tilde{\mathbf{E}}(t_k + T|t_k)\|^2_{\mathbf{G}}$, while the process cost is defined by $L_\Phi = \|\tilde{\mathbf{E}}(\tau|t_k)\|^2_{\mathbf{P}} + \|\tilde{\mathbf{U}}_e(\tau|t_k)\|^2_{\mathbf{Q}}$. Here, $\mathbf{G}, \mathbf{P} \in \mathbb{R}^{6\times6}$, $\mathbf{Q} \in \mathbb{R}^{3\times3}$ are positive definite weighting matrices. Then, an optimisation model established on the nominal model can be written as

$$\begin{aligned} \text{Find} \quad & \tilde{\boldsymbol{x}}^* = \tilde{\boldsymbol{x}}(\tau|t_k), \tilde{\boldsymbol{u}}^* = \tilde{\boldsymbol{u}}(\tau|t_k) \\ \text{minimize} \quad & J_\Phi(\tilde{\mathbf{E}}(t_k), \tilde{\mathbf{U}}_e(t_k)) \\ \text{subject to} \quad & \forall\tau \in [t_k, t_k + T] \\ & \boldsymbol{x}(t_k) \in \tilde{\boldsymbol{x}}(t_k|t_k) \oplus \mathbb{O}_e \\ & \dot{\tilde{\boldsymbol{x}}}(\tau) = f(\tilde{\boldsymbol{x}}(\tau), \tilde{\boldsymbol{u}}(\tau)) \\ & \tilde{\boldsymbol{x}}(\tau) \in \mathbb{X}_\omega^{\text{tube}} \\ & \tilde{\boldsymbol{u}}(\tau) \in \mathbb{U}_m^{\text{tube}} \\ & \tilde{\mathbf{E}}(t_k + T|t_k) \in \boldsymbol{\Omega}_\Phi^{\text{tube}} \end{aligned} \tag{10}$$

in which $\mathbb{O}_e$ stands for the state-variation tube region, where $\mathbb{X}_\omega^{\text{tube}} = \{\tilde{\boldsymbol{x}}_\omega : \|\tilde{\boldsymbol{x}}_\omega\| \leq \bar{x}_\omega^{\text{tube}}\}$ and $\mathbb{U}_m^{\text{tube}} = \{\tilde{\boldsymbol{u}} : \|\tilde{\boldsymbol{u}}\| \leq \bar{u}^{\text{tube}}\}$ are the tightened state and input constraints, respectively. $\boldsymbol{\Omega}_\Phi^{\text{tube}}$ is a terminal invariant set. Its definition is stated below.

Definition 1 *$\boldsymbol{\Omega}_\Phi^{tube}$ and $\tilde{\boldsymbol{u}}^f$ are recognised as the terminal invariant set and the corresponding terminal control law for the nominal tracking-error system (8), if condi-*

tions (11a)-(11c) can be satisfied when $\tilde{\mathbf{E}}$ *enters* $\mathbf{\Omega}_{\Phi}^{tube}$*:*

$$\begin{cases} \tilde{\boldsymbol{x}}(\tau|t_k) \in \mathbb{X}_{\omega}^{tube} & \text{(11a)} \\ \tilde{\boldsymbol{u}}^f(\tau|t_k) \in \mathbb{U}_m^{tube} & \text{(11b)} \\ L_{\Phi}(\tilde{\mathbf{E}}(\tau|t_k), \tilde{\mathbf{U}}_e(\tau|t_k)) + \dot{g}_{\Phi}(\tilde{\mathbf{E}}(\tau|t_k)) \leq 0 & \text{(11c)} \end{cases}$$

The tightened constraint/variable regions (e.g., $\mathbb{X}_{\omega}^{\text{tube}}$, $\mathbb{U}_m^{\text{tube}}$ and $\mathbb{O}_e$), along with the terminal invariant set $\mathbf{\Omega}_{\Phi}^{\text{tube}}$, can all be specified offline, which will be detailed in the next subsection.

3.3 Robust Control Law and Offline Parameter Designs

The next lemma (Lemma 2) gives the design of the terminal invariant set $\mathbf{\Omega}_{\Phi}^{\text{tube}}$ and the corresponding terminal controller $\tilde{\boldsymbol{u}}^f$ for the reentry-vehicle attitude-tracking system.

Lemma 2 *Define* $\mathbf{\Omega}_{\Phi}^{tube}$ *and* $\tilde{\boldsymbol{u}}^f$ *in the form of (12) and (14)*

$$\mathbf{\Omega}_{\Phi}^{tube} = \{\tilde{\mathbf{E}} : \|\tilde{\mathbf{E}}\|_{\mathbf{R}} \leq \epsilon\},\ \epsilon = \min\{\epsilon_1, \epsilon_2\} \tag{12}$$

with

$$\begin{cases} \epsilon_1 = \sqrt{\lambda_{min}(\mathbf{G})}(\bar{x}_{\omega}^{tube} - \bar{\Theta}_1) \\ \epsilon_2 = \sqrt{\lambda_{min}(\mathbf{G})}(\frac{\bar{u}^{tube} - (\bar{r}_0 \bar{I}' \bar{\Omega} \bar{I} \bar{r}_0' - \bar{r}_1)\bar{x}_{\omega}^{tube} - \bar{\Theta}_2}{\|\tilde{\mathbf{K}}\|}) \end{cases} \tag{13}$$

and

$$\tilde{\boldsymbol{u}}^f = -\dot{\boldsymbol{R}}(\tilde{\boldsymbol{\Theta}})\tilde{\boldsymbol{\omega}} + \boldsymbol{R}(\tilde{\boldsymbol{\Theta}})\boldsymbol{I}^{-1}\boldsymbol{\Omega}(\tilde{\boldsymbol{\omega}})\boldsymbol{I}\tilde{\boldsymbol{\omega}} + \tilde{\mathbf{K}}\tilde{\mathbf{E}} + \ddot{\mathbf{\Theta}}_r \tag{14}$$

where $\tilde{\mathbf{K}} = [\tilde{\mathbf{K}}_1, \tilde{\mathbf{K}}_2] \in \mathbb{R}^{3\times 6}$ *with* $\tilde{\mathbf{K}}_1 = \text{diag}\{\tilde{k}_{i1}\}_{i=1}^3$, $\tilde{k}_{i1} < 0$, $\tilde{\mathbf{K}}_2 = \text{diag}\{\tilde{k}_{i2}\}_{i=1}^3$, $\tilde{k}_{i2} < 0$ *and* $\tilde{k}_{i2}^2 + 4\tilde{k}_{i1} > 0$. *If* $\mathbf{G}$ *and* $\tilde{\mathbf{K}}$ *are selected such that (15) holds true, then* $\mathbf{\Omega}_{\Phi}^{tube}$ *and* $\tilde{\boldsymbol{u}}^f$ *can be recognised as the terminal invariant set and terminal control law, respectively, for the nominal reentry-vehicle attitude-tracking-error system (8).*

$$\mathbf{A}^T\mathbf{G} + \mathbf{G}\mathbf{A} + \tilde{\mathbf{K}}^T\mathbf{Q}\tilde{\mathbf{K}} + \mathbf{P} \leq \mathbf{0} \tag{15}$$

and the nominal attitude-tracking-error system (8) can be written as

$$\dot{\tilde{\mathbf{E}}} = \mathbf{A}\tilde{\mathbf{E}}$$

Here, $\mathbf{A}$ *is given by*

$$\mathbf{A} = \begin{bmatrix} \mathbf{0}_{3\times 3} & \mathbf{I}_3 \\ \tilde{\mathbf{K}}_1 & \tilde{\mathbf{K}}_2 \end{bmatrix} \in \mathbb{R}^{6\times 6}$$

PROOF. The proof contains three parts. First, based on the definition of $\tilde{\mathbf{E}}_{\theta}$ and $\tilde{\mathbf{E}}_{\omega}$, we have $\tilde{\boldsymbol{x}}_{\theta} = \tilde{\mathbf{E}}_{\theta} + \mathbf{\Theta}_r$ and $\tilde{\boldsymbol{x}}_{\omega} = \tilde{\mathbf{E}}_{\omega} + \dot{\mathbf{\Theta}}_r$. When the nominal state variable $\tilde{\boldsymbol{x}}$ enters $\mathbf{\Omega}_{\Phi}^{\text{tube}}$, the following inequality holds true

$$\begin{aligned} \|\tilde{\boldsymbol{x}}_{\omega}\| =& \|\tilde{\mathbf{E}}_{\omega} + \dot{\mathbf{\Theta}}_r\| \leq \|\tilde{\mathbf{E}}_{\omega}\| + \|\dot{\mathbf{\Theta}}_r\| \\ \leq& \|\tilde{\mathbf{E}}\| + \bar{\Theta}_1 \leq \frac{\|\tilde{\mathbf{E}}\|_{\mathbf{G}}}{\sqrt{\lambda_{\min}(\mathbf{G})}} + \bar{\Theta}_1 \leq \bar{x}_{\omega}^{\text{tube}} \end{aligned} \tag{16}$$

Hence, it is obvious that $\tilde{\boldsymbol{x}} \in \mathbb{X}_{\omega}^{\text{tube}}$.

Next, attention is given to $\tilde{\boldsymbol{u}}^f$. By analysing its norm bound, we have

$$\begin{aligned} \tilde{\boldsymbol{u}}^f =& \|\boldsymbol{R}(\tilde{\mathbf{\Theta}})\boldsymbol{I}^{-1}\boldsymbol{\Omega}(\tilde{\boldsymbol{\omega}})\boldsymbol{I}\tilde{\boldsymbol{\omega}}\| - \|\dot{\boldsymbol{R}}(\tilde{\mathbf{\Theta}})\tilde{\boldsymbol{\omega}}\| + \|\tilde{\mathbf{K}}\tilde{\mathbf{E}}\| + \|\ddot{\mathbf{\Theta}}_r\| \\ \leq& (\bar{r}_0\bar{I}'\bar{\Omega}\bar{I}\bar{r}_0' - \bar{r}_1)\bar{x}_{\omega}^{\text{tube}} + \bar{\Theta}_2 + \|\tilde{\mathbf{K}}\|\frac{\|\tilde{\mathbf{E}}\|_{\mathbf{G}}}{\sqrt{\lambda_{\min}(\mathbf{G})}} \leq \bar{u}^{\text{tube}} \end{aligned} \tag{17}$$

which implies that $\tilde{\boldsymbol{u}}^f(\tau|t_k) \in \mathbb{U}_m^{\text{tube}}$ is satisfied.

Finally, differentiating (9), one has

$$\begin{aligned} & L_{\Phi}(\tilde{\mathbf{E}}, \tilde{\mathbf{U}}_e) + \frac{dg_{\Phi}(\tilde{\mathbf{E}})}{dt} \\ &= L_{\Phi}(\tilde{\mathbf{E}}, \tilde{\mathbf{K}}\tilde{\mathbf{E}}) + \dot{g}_{\Phi}(\tilde{\mathbf{E}}) \\ &= \|\tilde{\mathbf{E}}\|_{\mathbf{P}}^2 + \|\tilde{\mathbf{K}}\tilde{\mathbf{E}}\|_{\mathbf{Q}}^2 + \dot{\tilde{\mathbf{E}}}^T\mathbf{G}\tilde{\mathbf{E}} + \tilde{\mathbf{E}}^T\mathbf{G}\dot{\tilde{\mathbf{E}}} \\ &= \tilde{\mathbf{E}}^T\mathbf{P}\tilde{\mathbf{E}} + \tilde{\mathbf{E}}^T\tilde{\mathbf{K}}^T\mathbf{Q}\tilde{\mathbf{K}}\tilde{\mathbf{E}} + \dot{\tilde{\mathbf{E}}}^T\mathbf{G}\tilde{\mathbf{E}} + \tilde{\mathbf{E}}^T\mathbf{G}\dot{\tilde{\mathbf{E}}} \\ &= \tilde{\mathbf{E}}^T(\mathbf{A}^T\mathbf{G} + \mathbf{G}\mathbf{A} + \tilde{\mathbf{K}}^T\mathbf{Q}\tilde{\mathbf{K}} + \mathbf{P})\tilde{\mathbf{E}} \end{aligned} \tag{18}$$

Note that in (18), $\tilde{\mathbf{K}}\tilde{\mathbf{E}}$ is obtained by substituting $\tilde{\boldsymbol{u}}^f$ back into $\tilde{\mathbf{U}}_e$. The term $\tilde{\boldsymbol{u}}^f$ is not substituted for $\tilde{\mathbf{E}}_{\omega}$, as the control only appears in the derivative of $\tilde{\mathbf{E}}_{\omega}$. The characteristic polynomial of the transcribed nominal attitude-tracking-error system can be written as

$$\lambda_A^2 - \tilde{k}_{i2}\lambda_A - \tilde{k}_{i1}, \quad i = \{1, 2, 3\}$$

Providing that $\tilde{k}_{i1}, \tilde{k}_{i2} < 0$, and $\tilde{k}_{i2}^2 + 4\tilde{k}_{i1} > 0$, the eigenvalues of $\mathbf{A}$ satisfy $\lambda_A = \frac{\tilde{k}_{i2} \pm \sqrt{\tilde{k}_{i2}^2 + 4\tilde{k}_{i1}}}{2} < 0$. Moreover, if $\mathbf{A}^T\mathbf{G} + \mathbf{G}\mathbf{A} + \tilde{\mathbf{K}}^T\mathbf{Q}\tilde{\mathbf{K}} + \mathbf{P} \leq 0$, then we have $L_{\Phi} + \dot{g}_{\Phi} \leq 0$. Consequently, based on Definition 1, $\mathbf{\Omega}_{\Phi}^{\text{tube}}$ and $\tilde{\boldsymbol{u}}^f$ given by (12) and (14) are the terminal invariant set and terminal control law for (8), respectively.

To ensure robust constraint satisfaction for all admissible uncertainties (e.g., actual system variables can satisfy (6)), a nonlinear feedback law should be designed. Let us define the deviation between the actual and nominal state variable as $O_e(\tau) = \boldsymbol{x}(\tau) - \tilde{\boldsymbol{x}}(\tau)$. Differentiating $O_e(\tau)$ results in

$$\begin{aligned} \dot{O}_e(\tau) =& \dot{\boldsymbol{x}}(\tau) - \dot{\tilde{\boldsymbol{x}}}(\tau) \\ =& \begin{pmatrix} \boldsymbol{x}_{\omega} - \tilde{\boldsymbol{x}}_{\omega} \\ \dot{\boldsymbol{R}}(\mathbf{\Theta})\boldsymbol{\omega} - \boldsymbol{R}(\mathbf{\Theta})\boldsymbol{I}^{-1}\boldsymbol{\Omega}(\omega)\boldsymbol{I}\boldsymbol{\omega} + \boldsymbol{u} + \mathbf{\Delta} - \dot{\boldsymbol{R}}(\tilde{\mathbf{\Theta}})\tilde{\boldsymbol{\omega}} + \\ \boldsymbol{R}(\tilde{\mathbf{\Theta}})\boldsymbol{I}^{-1}\boldsymbol{\Omega}(\tilde{\boldsymbol{\omega}})\boldsymbol{I}\tilde{\boldsymbol{\omega}} - \tilde{\boldsymbol{u}} \end{pmatrix} \end{aligned} \tag{19}$$

After obtaining the optimised solution $(\tilde{\boldsymbol{x}}^*, \tilde{\boldsymbol{u}}^*)$ at t_k, the actual control command $\boldsymbol{u}(\tau), \tau \in [t_k, t_k+1]$ can be designed in the form of

$$\begin{aligned}\boldsymbol{u}(\tau) =&\mathbf{K}O_e + \boldsymbol{R}(\boldsymbol{\Theta})\boldsymbol{I}^{-1}\boldsymbol{\Omega}(\omega)\boldsymbol{I}\boldsymbol{\omega} - \dot{\boldsymbol{R}}(\boldsymbol{\Theta})\boldsymbol{\omega} + \dot{\boldsymbol{R}}(\tilde{\boldsymbol{\Theta}}^*)\tilde{\boldsymbol{\omega}}^* \\ &- \boldsymbol{R}(\tilde{\boldsymbol{\Theta}}^*)\boldsymbol{I}^{-1}\boldsymbol{\Omega}(\tilde{\boldsymbol{\omega}}^*)\boldsymbol{I}\tilde{\boldsymbol{\omega}}^* + \tilde{\boldsymbol{u}}^*\end{aligned} \tag{20}$$

Similar to the expression of $\tilde{\mathbf{K}}$, $\mathbf{K}$ is defined as $\mathbf{K} = [\mathbf{K}_1, \mathbf{K}_2] \in \mathbb{R}^{3\times 6}$ with $\mathbf{K}_1 = \text{diag}\{k_{i1}\}_{i=1}^3, k_{i1} < 0, \mathbf{K}_2 = \text{diag}\{k_{i2}\}_{i=1}^3, k_{i2} < 0$ and $k_{i2}^2 + 4k_{i1} > 0$. In addition, $\mathbf{B}$ is defined as

$$\mathbf{B} = \begin{bmatrix} \mathbf{0}_{3\times 3} & \mathbf{I}_3 \\ \mathbf{K}_1 & \mathbf{K}_2 \end{bmatrix} \in \mathbb{R}^{6\times 6}.$$

Then, Lemma 3 can be established to provide indications on how to choose the tightened constraint/variable regions for the optimisation model (10) offline. It also shows that by using the feedback control law (20), the actual system variable can account (6) for all admissible uncertainties.

Lemma 3 *Given $\bar{x}_\omega^{tube}$ and $\bar{u}^{tube}$ in the form of*

$$\begin{cases} \bar{x}_\omega^{tube} = \bar{x}_\omega - \sqrt{3}\bar{\Delta}\bar{c}, \quad \bar{c} = \max\{\bar{c}_i\} \\ \bar{c}_i = G_i\left(\frac{\ln(\lambda_{i2}/\lambda_{i1})}{\lambda_{i1}-\lambda_{i2}}\right), \quad G_i(\tau) = \frac{e^{\lambda_{i2}\tau} - e^{\lambda_{i1}\tau}}{\sqrt{k_{i2}^2+4k_{i1}}} \\ \bar{u}^{tube} = \bar{u} - 2\bar{r}_0\bar{I}'\bar{\Omega}\bar{I}\bar{r}_0'\bar{x}_\omega + \sqrt{3}\bar{\Delta}\bar{c}(\bar{r}_1\bar{r}_0' + \bar{r}_0\bar{I}'\bar{\Omega}\bar{I}\bar{r}_0') \end{cases} \tag{21}$$

where $\lambda_B = \{\lambda_{i1}, \lambda_{i2}\}_{i=1}^3$ denotes the eigenvalues of matrix $\mathbf{B}$. If the feedback control law $\boldsymbol{u}(\tau)$ is applied to steer the actual reentry attitude dynamical system over $\tau \in [t_k, t_{k+1})$, then we obtain the following properties:

(1) The actual attitude variables can stay within a tube region $\boldsymbol{x}(\tau) \in \tilde{\boldsymbol{x}}^*(\tau|t_k) \oplus \mathbb{O}_e$;
(2) The actual attitude variables and control inputs can be constrained to their tolerable regions, i.e., $\boldsymbol{x} \in \mathbb{X}_\omega$ and $\boldsymbol{u} \in \mathbb{U}_m$.

PROOF. Substituting the feedback control law (20) into (19) results in

$$\dot{O}_e(\tau) = \mathbf{B}O_e(\tau) + \boldsymbol{\Delta}(\tau) \tag{22}$$

Integrating (22) with initial condition $O_e(\tau) = 0$, one can obtain the following inequality:

$$\begin{aligned} O_e(\tau) =& \int_0^t e^{\mathbf{B}(t-\tau)}\boldsymbol{\Delta}(\tau)d\tau \\ \leq& \mathbf{B}^{-1}|\boldsymbol{\Delta}(\tau)|\int_0^t |e^{\mathbf{B}(t-\tau)}|d\tau \end{aligned} \tag{23}$$

It is easy to calculate that

$$\mathbf{B}^{-1} = \begin{bmatrix} \mathbf{0}_{3\times 3} & \mathbf{I}_3 \\ \mathbf{K}_1' & \mathbf{K}_2' \end{bmatrix} \in \mathbb{R}^{6\times 6}$$

in which $\mathbf{K}_1' = \text{diag}\{1/k_{i1}\}_{i=1}^3$ and $\mathbf{K}_2' = \text{diag}\{-k_{i2}/k_{i1}\}_{i=1}^3$. To calculate the eigenvalue of $\mathbf{B}$, one has

$$|\lambda_B\mathbf{I}_6 - \mathbf{B}| = \begin{vmatrix} \mathbf{B}_1 & \mathbf{B}_2 \\ \mathbf{B}_3 & \mathbf{B}_4 \end{vmatrix} = 0$$

Here, $\mathbf{B}_1 = \text{diag}\{\lambda_B, \lambda_B, \lambda_B\}$, $\mathbf{B}_2 = \text{diag}\{-1, -1, -1\}$, $\mathbf{B}_3 = \text{diag}\{-k_{i1}\}_{i=1}^3$ and $\mathbf{B}_4 = \text{diag}\{\lambda_B - k_{i2}\}_{i=1}^3$. Since $\mathbf{B}_1\mathbf{B}_3 = \mathbf{B}_3\mathbf{B}_1$, we have

$$\begin{aligned} &|\mathbf{B}_1\mathbf{B}_4 - \mathbf{B}_2\mathbf{B}_3| \\ =& \begin{vmatrix} \lambda_B^2 - k_{12}\lambda_B - k_{11} & 0 & 0 \\ 0 & \lambda_B^2 - k_{22}\lambda_B - k_{21} & 0 \\ 0 & 0 & \lambda_B^2 - k_{32}\lambda_B - k_{31} \end{vmatrix} \end{aligned}$$

resulting in $\lambda_B = \{\lambda_{i1,2}\}_{i=1}^3 = \left\{\frac{k_{i2} \pm \sqrt{k_{i2}^2+4k_{i1}}}{2}\right\}_{i=1}^3$. Subsequently, (23) can be further written as

$$|O_e(\tau)| \leq \bar{\Delta} \cdot [\{F_i\}_{i=1}^3, \{G_i\}_i^3]^T \tag{24}$$

with

$$F_i(\tau) = \frac{(e^{\lambda_{i1}\tau} - 1)\lambda_{i2} - (e^{\lambda_{i2}\tau} - 1)\lambda_{i1}}{k_{i1}\sqrt{k_{i2}^2 + 4k_{i1}}} \tag{25}$$

By analysing the derivative of $F_i(\tau)$, one obtains $\frac{\partial F_i(\tau)}{\partial \tau} > 0$, indicating that $\max(F_i)(\tau) = \lim_{\tau\to\infty} F_i(\tau) = -\frac{1}{k_{i1}}$. For $G_i(\tau)$, it can be verified that $G_i(0) = G_i(\infty) = 0$. Based on Rolle's theorem, a maximum value of $G_i(\tau)$ can be achieved at the stationary point $\tau = \frac{\ln(\lambda_{i2}/\lambda_{i1})}{\lambda_{i1}-\lambda_{i2}}$. Therefore, (24) is further written as

$$|O_e(\tau)| \leq \bar{\Delta} \cdot \left[\{-1/k_{i1}\}_{i=1}^3, \{\bar{c}_i\}_{i=1}^3\right]^T \tag{26}$$

Then, the proof of (1) can be fulfilled by defining the state tube region as $\mathbb{O}_e = \{O_e \in \mathbb{R}^6 : |O_e| \leq \bar{\Delta}[\{-1/k_{i1}\}_{i=1}^3, \{\bar{c}_i\}_{i=1}^3]^T\}$.

To prove (2), the definition of $O_e(\tau)$ is recalled:

$$\begin{aligned} \|\boldsymbol{x}_\omega(\tau)\| =& \|O_\omega(\tau) + \tilde{\boldsymbol{x}}_\omega^*(\tau|t_k)\| \\ \leq& \|O_\omega(\tau)\| + \|\tilde{\boldsymbol{x}}_\omega^*(\tau|t_k)\| \\ \leq& \bar{x}_\omega^{\text{tube}} + \sqrt{3}\bar{c}\bar{\Delta} = \bar{x}_\omega \end{aligned} \tag{27}$$

where $O_\omega(\tau) = \boldsymbol{x}_\omega(\tau) - \tilde{\boldsymbol{x}}_\omega(\tau) \in \mathbb{R}^{3\times 1}$. (27) implies that the actual state constraint can be satisfied. That is, $\boldsymbol{x}_\omega \in \mathbb{X}_\omega$. For the actual input constraint, let us define two new variables

$$\begin{cases} \hat{\boldsymbol{u}}^* = \boldsymbol{u}^* + \dot{\boldsymbol{R}}(\boldsymbol{\Theta}^*)\boldsymbol{\omega}^* - \boldsymbol{R}(\boldsymbol{\Theta}^*)\boldsymbol{I}^{-1}\boldsymbol{\Omega}(\boldsymbol{\omega}^*)\boldsymbol{I}\boldsymbol{\omega}^* & \text{(28a)} \\ \hat{\boldsymbol{u}}^m = \boldsymbol{u} + \dot{\boldsymbol{R}}(\boldsymbol{\Theta})\boldsymbol{\omega} - \boldsymbol{R}(\boldsymbol{\Theta})\boldsymbol{I}^{-1}\boldsymbol{\Omega}(\boldsymbol{\omega})\boldsymbol{I}\boldsymbol{\omega} & \text{(28b)} \end{cases}$$

Note that $\boldsymbol{\omega} = \mathbf{G}(\boldsymbol{\Theta})\boldsymbol{x}_\omega$. From (20) and (28), it is clear that

$$\hat{\boldsymbol{u}}^a = \hat{\boldsymbol{u}}^* + \mathbf{B}O_e \tag{29}$$

Two sets are further defined as

$$\begin{cases} \hat{\mathbb{U}}_m^{\text{tube}} = \{\hat{\boldsymbol{u}}^* : \|\boldsymbol{u}^*\| \leq \bar{u}^{\text{tube}} + \bar{r}_1 \bar{r}_0^{'} \bar{x}_\omega^{\text{tube}} + \bar{r}_0 \bar{I}^{'} \bar{\Omega} \bar{I} \bar{r}_0^{'} \bar{x}_\omega^{\text{tube}}\} \\ \hat{\mathbb{U}}_m = \{\hat{\boldsymbol{u}}^m : \|\hat{\boldsymbol{u}}^m\| \leq \bar{u} + \bar{r}_1 \bar{r}_0^{'} \bar{x}_\omega - \bar{r}_0 \bar{I}^{'} \bar{\Omega} \bar{I} \bar{r}_0^{'} \bar{x}_\omega\} \end{cases} \tag{30a}$$

(30b)

By analysing $\mathbb{O}_e$, we have $\mathbf{B}\mathbb{O}_e \subset \{o \in \mathbb{R}^3 : \|o\| \leq \sqrt{3}\bar{\Delta}\bar{a}_c\}$, in which $\bar{a}_c = \arg\max_i (1 - k_{i2}\bar{c}_i)$. Based on the tightened bounds, it holds true that $\mathbf{B}\mathbb{O}_e \oplus \hat{\mathbb{U}}_m^{\text{tube}} \subset \hat{\mathbb{U}}_m$. Furthermore, by analysing the norm bound of (28), it can be obtained that $\hat{\boldsymbol{u}}^* \in \hat{\mathbb{U}}_m^{\text{tube}}$ and $\hat{\boldsymbol{u}}^m \in \hat{\mathbb{U}}_m$. Consequently, one can conclude that $\boldsymbol{u} \in \mathbb{U}_m$, which completes the proof.

Remark 2 *The terminal invariant set $\boldsymbol{\Omega}_\Phi^{tube}$ can be constructed in accordance with the definition of $\bar{x}_\omega^{tube}$ and $\bar{u}^{tube}$ provided in (21). It is noteworthy that by setting physically sensible constraint bounds (e.g., $\bar{x}_\omega$ and $\bar{u}$), both ϵ_1 and ϵ_2 in (13) can become non-negative.*

4 Main Theoretical Results

This section presents the main theoretical findings of the designed CRMPC-based attitude control algorithm.

4.1 Recursive Feasibility

In Theorem 1, the recursive feasibility of the proposed CRMPC optimisation process is established.

Theorem 1 *Given the attitude-tracking-error systems in the form of (5), if there exists a feasible control solution for the optimisation model (10) at time t_k, then the optimisation model will be recursively feasible for any $t_{k+1} > t_k$.*

PROOF. To begin with, attention is given to the attitude-tracking-error system (5) and the optimization model (10). Suppose it is able to find an optimized control solution $\tilde{\boldsymbol{u}}^*(\tau|t_k)$ by solving the optimization model (10). Then, the actual attitude dynamical system is steered via the robust control law (20) until τ reaches t_{k+1}. Now, our goal becomes to prove the existence of at least one candidate solution for the optimization model (10) at t_{k+1}. By combining the tail of $\tilde{\boldsymbol{u}}^*(\tau|t_k)$ and the terminal control law designed in Lemma 2, we can construct a candidate control sequence in the form of

$$\tilde{\boldsymbol{u}}(\tau|t_{k+1}) = \begin{cases} \tilde{\boldsymbol{u}}^*(\tau|t_k) & \text{if} \quad \tau \in [t_{k+1}, t_k + T) \\ \tilde{\boldsymbol{u}}^f(\tau|t_k) & \text{if} \quad \tau \in [t_k + T, t_{k+1} + T) \end{cases} \tag{31}$$

Note that $\tilde{\boldsymbol{u}}(\tau|t_{k+1})$ can be a feasible control solution for the optimization model (10) at time instant t_{k+1}. This is because according to Lemma 3, we have $\boldsymbol{x}(t_{k+1}) \in \tilde{\boldsymbol{x}}^*(t_{k+1}|t_k) \oplus \mathbb{O}_e$, implying that $\tilde{\boldsymbol{x}}(t_{k+1}) = \tilde{\boldsymbol{x}}^*(t_{k+1}|t_k)$ is a feasible initial system state vector for the optimization model (10) at t_{k+1}. Moreover, it is clear that applying $\tilde{\boldsymbol{u}}(\tau|t_{k+1})$ can steer $\tilde{\mathbf{E}}(\tau|t_{k+1})$ into $\boldsymbol{\Omega}_\Phi^{\text{tube}}$ for $\tau \in [t_{k+1}, t_k + T)$ without violating the state and control tube constraints. According to Lemma 2, we have $\tilde{\mathbf{E}}(\tau|t_{k+1}) \in \boldsymbol{\Omega}_\Phi^{\text{tube}}$ under the terminal control $\tilde{\boldsymbol{u}}(\tau|t_{k+1})$ over $[t_k + T, t_{k+1} + T)$, indicating that $\tilde{\boldsymbol{x}}_\omega(\tau|t_{k+1}) \in \mathbb{X}_\omega^{\text{tube}}$ and $\tilde{\boldsymbol{u}}(\tau|t_{k+1}) \in \mathbb{U}_m^{\text{tube}}$. As a consequence, $\tilde{\boldsymbol{u}}(\tau|t_{k+1})$ is a feasible solution for (10) at t_{k+1}. By induction, the entire proof can be completed.

Remark 3 *The initial feasibility of the optimisation problem (10) must be carefully considered. Note that once the terminal region constraint $\tilde{\mathbf{E}}(t_k + T|t_k) \in \boldsymbol{\Omega}_\Phi^{tube}$ is constructed via (12) and (13), a proper value of predictive horizon T should then be assigned. A small T can decrease the computational time required for the optimisation process, while a large predictive horizon T can be applied to enlarge the region of attraction, thereby ensuring the optimisation model is feasible at $t_k = 0$. However, this will inevitably result in high computational load. Therefore, a balanced T should be determined offline for practical applications.*

4.2 ISS stability

Theorem 2 illustrates the ISS of using the proposed CRMPC scheme to steer the reentry-vehicle attitude-tracking system.

Theorem 2 *At time point t_k, if the optimisation model (10) is feasible, then using the proposed CRMPC control scheme to steer the reentry-vehicle attitude-tracking system is ISS.*

PROOF. Let us chose $V_\phi = J_\Phi(\tilde{\mathbf{E}}^*(t_k), \tilde{\mathbf{U}}_e^*(t_k))$ as the Lyapunov function for the attitude-tracking-error system. By analysing the difference of V_ϕ at t_{k+1} and t_k, one can obtain the following inequality:

$$\begin{aligned} & V_\phi(t_{k+1}) - V_\phi(t_k) \\ & = J_\Phi(\tilde{\mathbf{E}}^*(t_{k+1}), \tilde{\mathbf{U}}_e^*(t_{k+1})) - J_\Phi(\tilde{\mathbf{E}}^*(t_k), \tilde{\mathbf{U}}_e^*(t_k)) \\ & \leq J_\Phi(\tilde{\mathbf{E}}(t_{k+1}), \tilde{\mathbf{U}}_e(t_{k+1})) - J_\Phi(\tilde{\mathbf{E}}^*(t_k), \tilde{\mathbf{U}}_e^*(t_k)) \\ & = \|\tilde{\mathbf{E}}(t_{k+1} + T|t_{k+1})\|_{\mathbf{G}}^2 - \|\tilde{\mathbf{E}}^*(t_k + T|t_k)\|_{\mathbf{G}}^2 \\ & - \int_{t_k}^{t_k+T} (\|\tilde{\mathbf{E}}^*(\tau|t_k)\|_{\mathbf{P}}^2 + \|\tilde{\mathbf{U}}_e^*(\tau|t_k)\|_{\mathbf{Q}}^2) d\tau \\ & + \int_{t_{k+1}}^{t_{k+1}+T} (\|\tilde{\mathbf{E}}(\tau|t_{k+1})\|_{\mathbf{P}}^2 + \|\tilde{\mathbf{U}}_e(\tau|t_{k+1})\|_{\mathbf{Q}}^2) d\tau \\ & = \|\tilde{\mathbf{E}}(t_{k+1} + T|t_{k+1})\|_{\mathbf{G}}^2 - \|\tilde{\mathbf{E}}^*(t_k + T|t_k)\|_{\mathbf{G}}^2 \\ & + \int_{t_{k+1}}^{t_k} (\|\tilde{\mathbf{E}}^*(\tau|t_k)\|_{\mathbf{P}}^2 + \|\tilde{\mathbf{U}}_e^*(\tau|t_k)\|_{\mathbf{Q}}^2) d\tau \\ & + \int_{t_k+T}^{t_{k+1}+T} (\|\tilde{\mathbf{E}}(\tau|t_{k+1})\|_{\mathbf{P}}^2 + \|\tilde{\mathbf{U}}_e(\tau|t_{k+1})\|_{\mathbf{Q}}^2) d\tau \end{aligned} \tag{32}$$

In (32), $J_\Phi(\tilde{\mathbf{E}}(t_{k+1}), \tilde{\mathbf{U}}_e(t_{k+1}))$ can be recognized as the objective value of $\tilde{\boldsymbol{u}}(\tau|t_{k+1})$ established in (31). From Lemma 2, one can obtain $\dot{g}_\Phi(\tilde{\mathbf{E}}) + L_\Phi(\tilde{\mathbf{E}}, \tilde{\mathbf{U}}_e) \leq 0$. Then, by integrating this equation over the time period $[t_k + T, t_{k+1} + T]$ and substituting the resulting equation into (32), it is easy to verify that $V_\phi(t_{k+1}) - V_\phi(t_k) \leq 0$. Accordingly, $\tilde{\mathbf{E}}$ will asymptotically converge to the origin, implying that there exists a $\mathcal{K}$ function such that for any $t > 0$, $\|\tilde{\mathbf{E}}^*(t)\| \leq \mathcal{K}(\mathbf{E}^*(0), t)$. As $O_e(t) \in \mathbb{O}_e$, there also exists a $\mathcal{K}_\infty$ function such that $\|O_e(t)\| \leq \mathcal{K}_\infty(\Delta)$. Hence, we have for any $t > 0$, $\|\mathbf{E}(t)\| \leq \mathcal{K}_\infty(\Delta) + \mathcal{K}(\mathbf{E}^*(0), t)$, which means the actual attitude tracking error system is input-to-state stable. This completes the proof.

5 Performance Verification

5.1 Parameter/Experiment Specification

This section validates the effectiveness of using the designed CRMPC scheme to address the noise-perturbed attitude-tracking-control problem. Reentry-dynamics-related parameters are assigned as follows. The components of $\boldsymbol{I}$ are $I_{xx} = 588791\text{kg} \cdot \text{m}^2$, $I_{xz} = 24242\text{kg} \cdot \text{m}^2$, $I_{yy} = 1303212\text{kg} \cdot \text{m}^2$, and $I_{zz} = 1534163\text{kg} \cdot \text{m}^2$. The initial conditions of the reentry vehicle are set to $\boldsymbol{\Theta} = [7.5°, 10°, -30°]^T$, and $\boldsymbol{\omega} = [0°/\text{s}, 0°/\text{s}, and 0°/\text{s}]^T$. System state and control constraints are specified as $\boldsymbol{\omega} \in \{\boldsymbol{\omega} : \|\boldsymbol{\omega}\| \leq 5°/\text{s}\}$ and $\mathbf{m} \in \{\mathbf{m} : \|\mathbf{m}\| \leq 1.356 \times 10^5 \text{N-m}\}$. $\boldsymbol{\Delta}$ is considered as the white noise bounded by $|\boldsymbol{\Delta}| \leq 2°/\text{s}$.

Furthermore, it is assumed that the inertia matrix has some uncertainties. Therefore, we set $\boldsymbol{I} = \boldsymbol{I} + \boldsymbol{\Delta}_I$ with $\boldsymbol{\Delta}_I = 5\%\boldsymbol{I}$. A nonlinear attitude tracking scenario is considered in the test where $\boldsymbol{\Theta}_r = [\alpha_r, \beta_r, \sigma_r]^T$ is given by $\beta_r = 0$ and:

$$\alpha_r(t) = \begin{cases} 10 + 2.5\sin(\frac{t}{2}), & \text{if } t \leq 25; \\ 10 + 0.5\cos(\frac{t}{4}), & \text{if } t > 25. \end{cases}$$

$$\sigma_r(t) = \begin{cases} -30 + 5\cos(\frac{t}{2}), & \text{if } t \leq 25; \\ -30 + 0.5\sin(\frac{t}{4}), & \text{if } t > 25. \end{cases}$$

Regarding the weighting matrices, $\mathbf{P}$ and $\mathbf{Q}$ are chosen as $\mathbf{P} = \text{diag}\{50, 50, 50, 50, 50, 50\}$ and $\mathbf{Q} = \text{diag}\{10, 10, 10\}$. $\tilde{\mathbf{K}}$=$[\tilde{\mathbf{K}}_1, \tilde{\mathbf{K}}_2]$ and $\mathbf{K}$=$[\mathbf{K}_1, \mathbf{K}_2]$, where $\tilde{\mathbf{K}}_1, \tilde{\mathbf{K}}_2 = \text{diag}\{-5, -5, -5\}, \mathbf{K}_1, \mathbf{K}_2 = \text{diag}\{-5, -5, -5\}$, respectively. According to Lemma 2, $\mathbf{G}$ is assigned as

$$\mathbf{G} = \begin{bmatrix} 80 & 0 & 0 & 30 & 0 & 0 \\ 0 & 80 & 0 & 0 & 30 & 0 \\ 0 & 0 & 80 & 0 & 0 & 30 \\ 30 & 0 & 0 & 36 & 0 & 0 \\ 0 & 30 & 0 & 0 & 36 & 0 \\ 0 & 0 & 30 & 0 & 0 & 36 \end{bmatrix}$$

Other parameters of CRMPC are specified as $\bar{r}_0 = 1.0846$, $\bar{r}_1 = 0.0873$, $\bar{r}_0^{'} = 1$, $\bar{\Omega} = 0.1511$, $\bar{I} \cdot \bar{I}^{'} = 2.6094$, $\bar{c} = 0.0835$, $\epsilon_1 = 0.2096$, and $\epsilon_2 = 0.0770$, respectively.

To conduct the experimental tests, a hardware-in-the-loop (HIL) platform is employed and visualised in Fig. 1. The working principle of the HIL platform is demonstrated in Fig. 2. The experimental platform mainly consists of three components:

- A reentry-vehicle model simulator (NI PXI-6723 D/A converting module, NI PXIe-8820 2.2 GHz Celeron 1020E Dual-Core and PXI-6224 A/D converting module);
- A controller unit (PCI-1723-BE D/A converting module and ADVANTECH 610L with I5-8500/4G/1TB);
- An inertial measurement unit (IMU) and a 3-axis rotating platform.

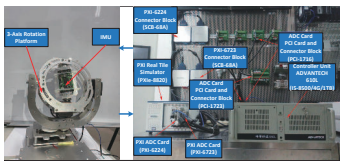

Fig. 1. Experimental platform.

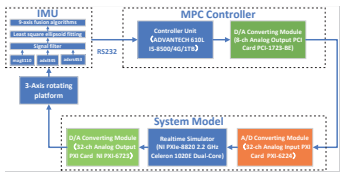

Fig. 2. Working principle of the HIL platform.

As shown in Fig. 2, the attitude dynamical model of the reentry vehicle runs on the NI PXI real-time controller with NI LabVIEW real-time module version 8.0. The D/A converting module is applied by the controller to drive the 3-axis rotating platform. The attitude variables (angle of attack, sideslip and bank angles, and roll, pitch, and yaw angular rates) obtained via the IMU are provided to the controller unit to generate the proposed control law via RS232. Note that for aerospace-scale practical verification, it is necessary to consider measurement noises in the experiments, whilst some signal processing should be performed with respect to the sensor outputs. Specifically, we first apply a low-pass signal filter to the sensor outputs. Subsequently, the least-squares ellipsoid-fitting calibration algorithm, followed by a nine-axis fu-

sion method [11] will be triggered such that the negative effects caused by measurement noise can be alleviated.

Two experiments analysing other attitude tracking control algorithms were performed as a comparison against the proposed method. The first method was the standard linear quadratic regulator (LQR), which can be regarded as an unconstrained version of MPC. The second method analysed was a multirate MPC design proposed in [2]. For simplicity, we denote this double-layered approach as DLMPC in this section. Both DLMPC and CRMPC belong to the class of MPC-oriented tracking control strategies. However, the main reason for selecting this multirate controller for the comparison was that the results and analysis presented by [2] confirmed that the DLMPC has the capability to produce promising attitude-tracking results in the presence of external disturbances, whilst maintaining an acceptable real-time performance.

The DLMPC controller is defined by first separating the attitude dynamical system into two subsystems: an attitude-angle subsystem and an angular-rate subsystem. Then, it employs a compound double-layered control strategy, including an outer MPC-based attitude-angle control loop and an inner terminal sliding-mode control (TSMC)-based angular-rate control loop. Hence, the entire control process of this approach is separated into two different timescales, while the proposed CRMPC determines all the manipulated variables in a single control loop. Compared to the CRMPC, four additional parameters (i.e., $[q, p, \Gamma, \rho]$=$[5, 5, 0.15, 0.7]$) are included in the DLMPC to form the nonsingular continuous sliding manifold. The notations of these additional algorithm-related parameters follow the same definition as in the original paper, and their determination is mainly based on the designer's experience and experimental trials. The prediction horizon for CRMPC is set to $T = 20$s, and the sampling period is 0.2 s (5 Hz). As for the multirate controller, the outer layer is executed at a relatively slow control frequency to optimise the attitude-angle tracking performance, whereas the inner layer is subjected to a relatively fast frequency to achieve the tracking of angular rate commands. More precisely, the control frequency and prediction horizon are set to 0.2 s (5 Hz) and $T_{\mathrm{o}} = 20$ s for the outer layer. For the inner layer, a 0.04 s (25 Hz) control frequency and $T_{\mathrm{i}} = 30$ s prediction horizon are used.

5.2 Attitude-Tracking Results and Discussion

Fig. 3 presents the angular tracking trajectories as well as the tracking-error-evolution profiles. The angular rate profiles are depicted in Fig. 4, whilst the corresponding control moment results are shown in Fig. 5.

It can be seen from Fig. 3 5 that the proposed CRMPC algorithm is able to fulfill the tracking task in the presence of system constraints, uncertainties, and sensor

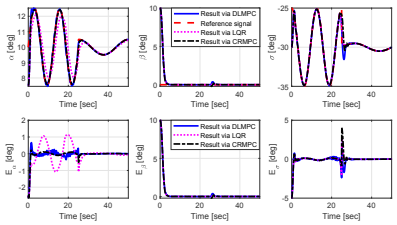

Fig. 3. Angular tracking and tracking error profiles obtained via DLMPC [2], CRMPC and LQR.

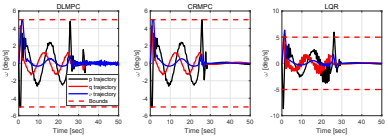

Fig. 4. Angular-rate-evolution profiles obtained via DLMPC [2], CRMPC, and LQR.

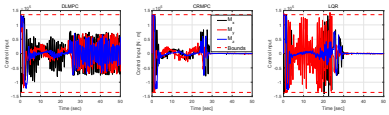

Fig. 5. Control-evolution profiles obtained via DLMPC [2], CRMPC, and LQR.

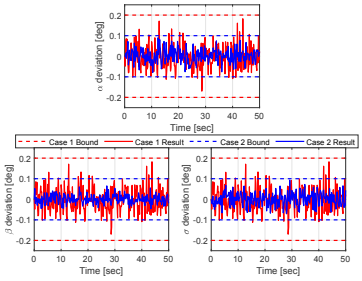

Fig. 6. CRMPC results: State deviation profiles for cases 1 and 2.

noises. Specifically, the actual angular profile $\boldsymbol{\Theta}$ can follow the desired reference $\boldsymbol{\Theta}_r$ with $\boldsymbol{\omega}$ and $\mathbf{m}$ always staying within their allowable regions (indicated by the red dashed lines in Fig. 4 and Fig. 5). This can be attributed to the application of tightened state/input constraints in the optimisation model and the designed robust nonlinear feedback law.

According to Lemma 3, the deviation between the nominal and actual attitude-angle trajectories $\boldsymbol{\Theta}_e = [\alpha_e, \beta_e, \sigma_e]^T$ should lie in a tube region. To clearly present this point, we design a case study by setting $\mathbf{K}_{\text{case 1}} = [\text{diag}\{-5, -5, -5\}, \text{diag}\{-5, -5, -5\}]$ and $\mathbf{K}_{\text{case 2}} = [\text{diag}\{-10, -10, -10\}, \text{diag}\{-10, -10, -10\}]$, respectively. The corresponding tube regions are as

follows:

$$\{\boldsymbol{\Theta}_e^{\text{case 1}} \in \mathbb{R}^3 : |\boldsymbol{\Theta}_e^{\text{case 1}}| \leq [0.2, 0.2, 0.2]\}$$
$$\{\boldsymbol{\Theta}_e^{\text{case 2}} \in \mathbb{R}^3 : |\boldsymbol{\Theta}_e^{\text{case 2}}| \leq [0.1, 0.1, 0.1]\}$$

Fig. 6 illustrates the evolution trajectories of $\boldsymbol{\Theta}_e$, in which it is obvious that CRMPC is capable of keeping the deviation value between the lower and upper tube bounds. Consequently, the effectiveness of applying the proposed CRMPC to track the desired attitude-angle signals can be verified.

As for the comparative experiments, the trajectory tracking results together with the control solutions are presented in Figs. 3-5. From these figures, we observe that although DLMPC can offer feasible tracking solutions, the corresponding tracking trajectories are relatively uneven with more oscillations. These phenomena become more noticeable in the angular rate and control profiles owing to the implementation of the inner TSMC controller. On the other hand, the proposed CRMPC method is able to achieve a better tracking performance in comparison to its counterpart, as the desired attitude-angle profiles can be smoothly tracked in a shorter time. In addition, CRMPC is able to rapidly steer the tracking error $\mathbf{E}_\theta$ closer towards the origin in the presence of uncertainties. In addition, as shown in Fig. 3, the tracking performance of LQR is poorer than that of CRMPC. This performance degradation can be attributed to the negative effects caused by the disturbances. More importantly, constraint violations are detected from the angular rate and control moment profiles (see e.g., Fig. 4 and Fig. 5), which means the tracking results produced by LQR cannot be recognised as feasible solutions.

To quantify the attitude-tracking performance of using DLMPC and CRMPC, two indicators are defined:

$$\text{EMS}(\mathbf{E}_\theta(t)) = \sqrt{\frac{1}{N_e}\sum_{k=1}^{N_e} \|\mathbf{E}_\theta(t_k)\|^2}$$
$$\text{CMS}(\mathbf{m}(t)) = \sqrt{\frac{1}{N_e}\sum_{k=1}^{N_e} \|\frac{\mathbf{m}(t_k)}{\bar{M}}\|^2}$$

where N_e denotes the total execution step. We apply the tracking error-mean-square (EMS) value $\text{EMS}(\mathbf{E}_\theta(t))$ and $\text{CMS}(\mathbf{m}(t))$ to evaluate the trajectory-tracking performance as well as the required control efforts. Note that when calculating $\text{CMS}(\mathbf{m}(t))$, the control moment $\mathbf{m}$ at each time step is scaled by its upper bound value.

Table 1
Assessment of the two methods

	DLMPC [2]	CRMPC
$\text{EMS}(\mathbf{E}_\theta(t))$	1.8193	1.6055 (↓11.75%)
$\text{CMS}(\mathbf{m}(t))$	0.5399	0.3552 (↓34.21%)

The obtained results are tabulated in Table I, which further confirms that CRMPC is able to achieve a better trajectory tracking performance than DLMPC. As evidence, the EMS and CMS values obtained using the CRMPC method are remarkably lower than those obtained using the DLMPC method (by 11.75% and 34.21%, respectively).

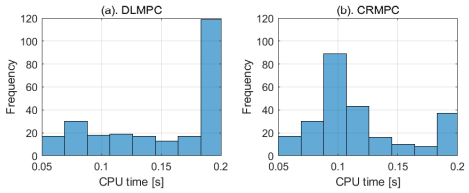

Fig. 7. Execution time distribution: (a) DLMPC [2]; (b) CRMPC.

As an important indicator to reflect the computational complexity, the time required for addressing the MPC optimisation model at each sample time is recorded and used to compare the two MPC-based attitude-tracking schemes. The average execution time t_{exe} resulting from CRMPC is calculated to be 0.1168 s, which is much lower than that of DLMPC (0.1527 s). The corresponding frequency distribution is illustrated in Fig. 7, where it is obvious that with the application of CRMPC, an unexpectedly high execution time is less likely to occur.

6 Conclusion

With a centralised structure, the proposed CRMPC scheme for tracking reference attitude trajectories of reentry vehicles successfully avoids additional controller development and parameter tuning of the inner angular-rate control loop. A nonlinear feedback law, together with the constraint-tightening strategy, has been developed so as to guarantee robust satisfaction of state/input constraints against external uncertainties. Meanwhile, by establishing a terminal controller and a corresponding terminal region, both recursive feasibility and input-to-state stability of the CRMPC algorithm are ensured. According to the HIL experimental results, we have found that by applying the proposed CRMPC scheme, a stable and convergent attitude-tracking process can be obtained. Furthermore, the merits of the proposed CRMPC strategy in comparison to two other typical control methods have been testified.

References

[1] Axler, S. (2015). *Eigenvalues, Eigenvectors, and Invariant Subspaces*, pages 131–161. Springer International Publishing, Cham.

[2] Bayat, F. (2019). Model predictive sliding control for finite-time three-axis spacecraft attitude tracking. *IEEE Transactions on Industrial Electronics*, 66(10):7986–7996.

[3] Cao, L. and Xiao, B. (2019). Exponential and resilient control for attitude tracking maneuvering of spacecraft with actuator

uncertainties. *IEEE/ASME Transactions on Mechatronics*, 24(6):2531–2540.

[4] Capello, E., Punta, E., Dabbene, F., Guglieri, G., and Tempo, R. (2017). Sliding-mode control strategies for rendezvous and docking maneuvers. *Journal of Guidance, Control, and Dynamics*, 40(6):1481–1487.

[5] Chai, R., Tsourdos, A., Savvaris, A., Xia, Y., and Chai, S. (2020). Real-time reentry trajectory planning of hypersonic vehicles: A two-step strategy incorporating fuzzy multiobjective transcription and deep neural network. *IEEE Transactions on Industrial Electronics*, 67(8):6904–6915.

[6] Dong, H., Hu, Q., and Akella, M. R. (2017). Safety control for spacecraft autonomous rendezvous and docking under motion constraints. *Journal of Guidance, Control, and Dynamics*, 40(7):1680–1692.

[7] Gao, J., Fu, Z., and Zhang, S. (2019). Adaptive fixed-time attitude tracking control for rigid spacecraft with actuator faults. *IEEE Transactions on Industrial Electronics*, 66(9):7141–7149.

[8] Guo, Z., Chang, J., Guo, J., and Zhou, J. (2018). Adaptive twisting sliding mode algorithm for hypersonic reentry vehicle attitude control based on finite-time observer. *ISA Transactions*, 77:20–29.

[9] Hegrenæs, Ø., Gravdahl, J. T., and Tøndel, P. (2005). Spacecraft attitude control using explicit model predictive control. *Automatica*, 41(12):2107–2114.

[10] Li, Z., Jing, X., Sun, B., and Yu, J. (2020). Autonomous navigation of a tracked mobile robot with novel passive bio-inspired suspension. *IEEE/ASME Transactions on Mechatronics*, 25(6):2633–2644.

[11] Lin, P., Lu, J., Tsai, C., and Ho, C. (2012). Design and implementation of a nine-axis inertial measurement unit. *IEEE/ASME Transactions on Mechatronics*, 17(4):657–668.

[12] Mammarella, M., Lee, D. Y., Park, H., Capello, E., Dentis, M., and Guglieri, G. (2019). Attitude control of a small spacecraft via tube-based model predictive control. *Journal of Spacecraft and Rockets*, 56(6):1662–1679.

[13] Mammarella, M., Lorenzen, M., Capello, E., Park, H., Dabbene, F., Guglieri, G., Romano, M., and Allgöwer, F. (2020). An offline-sampling smpc framework with application to autonomous space maneuvers. *IEEE Transactions on Control Systems Technology*, 28(2):388–402.

[14] Mao, Q., Dou, L., Yang, Z., Tian, B., and Zong, Q. (2020). Fuzzy disturbance observer-based adaptive sliding mode control for reusable launch vehicles with aeroservoelastic characteristic. *IEEE Transactions on Industrial Informatics*, 16(2):1214–1223.

[15] Nicolis, D., Allevi, F., and Rocco, P. (2020). Operational space model predictive sliding mode control for redundant manipulators. *IEEE Transactions on Robotics*, 36(4):1348–1355.

[16] Picasso, B., De Vito, D., Scattolini, R., and Colaneri, P. (2010). An mpc approach to the design of two-layer hierarchical control systems. *Automatica*, 46(5):823–831.

[17] Saad, A., Youssef, T., Elsayed, A. T., Amin, A., Abdalla, O. H., and Mohammed, O. (2019). Data-centric hierarchical distributed model predictive control for smart grid energy management. *IEEE Transactions on Industrial Informatics*, 15(7):4086–4098.

[18] Sirmatel, I. I. and Geroliminis, N. (2018). Economic model predictive control of large-scale urban road networks via perimeter control and regional route guidance. *IEEE Transactions on Intelligent Transportation Systems*, 19(4):1112–1121.

[19] Su, B., Zhang, F., and Huang, P. (2021). Robust control of triangular tethered satellite formation with unmeasured velocities. *Acta Astronautica*, 186:190–202.

[20] Tian, B., Fan, W., Su, R., and Zong, Q. (2015). Real-time trajectory and attitude coordination control for reusable launch vehicle in reentry phase. *IEEE Transactions on Industrial Electronics*, 62(3):1639–1650.

[21] Würth, L., Hannemann, R., and Marquardt, W. (2011). A two-layer architecture for economically optimal process control and operation. *Journal of Process Control*, 21(3):311–321.

[22] Yan, H., Tan, S., and He, Y. (2017). A small-gain method for integrated guidance and control in terminal phase of reentry. *Acta Astronautica*, 132:282–292.

[23] Zhang, J., Ma, K., Meng, G., and Tian, S. (2015). Spacecraft maneuvers via singularity-avoidance of control moment gyros based on dual-mode model predictive control. *IEEE Transactions on Aerospace and Electronic Systems*, 51(4):2546–2559.

[24] Zhou, B. (2019). On stability and stabilization of the linearized spacecraft attitude control system with bounded inputs. *Automatica*, 105:448–452.

[25] Zou, A. and Fan, Z. (2020). Fixed-time attitude tracking control for rigid spacecraft without angular velocity measurements. *IEEE Transactions on Industrial Electronics*, 67(8):6795–6805.

Attitude tracking control for reentry vehicles using centralised robust model predictive control

Chai, Runqi

2022-09-02

Chai R, Tsourdos A, Gao H, et al., (2022) Attitude tracking control for reentry vehicles using centralised robust model predictive control. Automatica, Volume 145, November 2022, Article number 110561

https://doi.org/10.1016/j.automatica.2022.110561